

MIT Open Access Articles

*Nonlinear characterization of GeSbS
chalcogenide glass waveguides*

The MIT Faculty has made this article openly available. **Please share** how this access benefits you. Your story matters.

Citation: Choi, Ju Won et al. "Nonlinear Characterization of GeSbS Chalcogenide Glass Waveguides." Scientific Reports 6.1 (2016): n. pag.

As Published: <http://dx.doi.org/10.1038/srep39234>

Publisher: Nature Publishing Group

Persistent URL: <http://hdl.handle.net/1721.1/108756>

Version: Final published version: final published article, as it appeared in a journal, conference proceedings, or other formally published context

Terms of use: Creative Commons Attribution-NonCommercial-NoDerivs License



SCIENTIFIC REPORTS



OPEN

Nonlinear characterization of GeSbS chalcogenide glass waveguides

Ju Won Choi^{1,*}, Zhaohong Han^{2,*}, Byoung-Uk Sohn¹, George F. R. Chen¹, Charmayne Smith³, Lionel C. Kimerling², Kathleen A. Richardson³, Anuradha M. Agarwal^{2,4} & Dawn T. H. Tan¹

Received: 30 August 2016
Accepted: 11 November 2016
Published: 21 December 2016

GeSbS ridge waveguides have recently been demonstrated as a promising mid – infrared platform for integrated waveguide – based chemical sensing and photodetection. To date, their nonlinear optical properties remain relatively unexplored. In this paper, we characterize the nonlinear optical properties of GeSbS glasses, and show negligible nonlinear losses at 1.55 μm . Using self – phase modulation experiments, we characterize a waveguide nonlinear parameter of $7\text{W}^{-1}/\text{m}$ and nonlinear refractive index of $3.71 \times 10^{-18}\text{m}^2/\text{W}$. GeSbS waveguides are used to generate supercontinuum from 1280 nm to 2120 nm at the –30 dB level. The spectrum expands along the red shifted side of the spectrum faster than on the blue shifted side, facilitated by cascaded stimulated Raman scattering arising from the large Raman gain of chalcogenides. Fourier transform infrared spectroscopic measurements show that these glasses are optically transparent up to 25 μm , making them useful for short – wave to long – wave infrared applications in both linear and nonlinear optics.

Waveguides based on chalcogenide glasses have seen great strides for both linear and nonlinear applications. Particularly significant because their band gap energies lie within the visible and near – infrared, many chalcogenide glasses have the advantage of a negligible two photon coefficient at the 1.55 μm wavelength. When combined with a relatively large nonlinear refractive index, chalcogenide glasses provide a promising means towards high efficiency nonlinear optical signal processing applications. As a consequence of its large optical nonlinearity, Kerr – based all – optical processes which have an intrinsic response time of less than 100 fs can be implemented very efficiently in chalcogenide glasses^{1,2}. The high photosensitivity resulting from the inherent structural flexibility in chalcogenide glasses enables its utilization in writing Bragg gratings in fiber as well as waveguides³. As a result of the aforementioned qualities, chalcogenide glasses are highly promising for all – optical signal processing such as switching, wavelength conversion and regeneration^{4–7}.

Chalcogenide glasses consist of the chalcogen elements (group 16 in the periodic table) such as sulfur (S), selenium (Se), and tellurium (Te), combined with network – forming elements such as silicon (Si), arsenic (As), germanium (Ge), phosphorus (P) and antimony (Sb). Therefore, the properties of chalcogenides such as their refractive indices, band – edges, and nonlinearity can be tuned according to its composition. Chalcogenide glasses are reported to get higher nonlinear optical properties than oxide glasses due to low vibrational energies of bonds induced by heavy chalcogen atoms. It enables their optical transparencies to extend up to mid – IR wavelength ranges. The glass density is also larger than that in oxide glasses that result in larger linear refractive index of 2–3. The optical merits such as wide transparency and large refractive index facilitate strong mode confinement and complete bandgap engineering for photonic devices. In particular, Ge – based glasses bonded with heavy metal oxide (e.g. Sb) create smaller multiphoton spectra for laser and fiber optic applications, therefore, ternary Ge – Sb – S system (GeSbS) has been widely investigated by its compositional dependence⁸. $\text{Ge}_{23}\text{Sb}_7\text{S}_{70}$ has been proven as one of promising waveguide materials because of low toxicity compared to As – based chalcogenide glasses^{9–11}. In addition, thermally evaporated $\text{Ge}_{23}\text{Sb}_7\text{S}_{70}$ films do not change much after alpha irradiation due to relatively high degree of radiation hardness¹². In this way, $\text{Ge}_{23}\text{Sb}_7\text{S}_{70}$ film has been deposited on a silica

¹Photonics Devices and System Group, Engineering Product Development, Singapore University of Technology and Design, 8 Somapah Rd. Singapore, 487372, Singapore. ²Department of Materials Science and Engineering, Massachusetts Institute of Technology, Cambridge, Massachusetts 02139, USA. ³College of Optics and Photonics, University of Central Florida, Orlando, Florida 32816, USA. ⁴Materials Processing Center, Massachusetts Institute of Technology, Cambridge, Massachusetts 02139, USA. *These authors contributed equally to this work. Correspondence and requests for materials should be addressed to D.T.H.T. (email: dawn_tan@sutd.edu.sg)

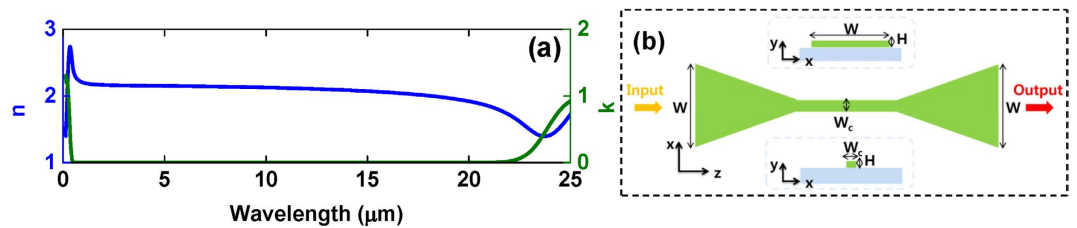


Figure 1. (a) Measured n and k values for $\lambda = 130\text{ nm}–25\ \mu\text{m}$ and (b) Schematic of GeSbS chalcogenide waveguide (Sky color: SiO_2 substrate, light green color: $\text{Ge}_{23}\text{Sb}_7\text{S}_{70}$ film).

substrate to fabricate ridge waveguides using photolithography and lift-off, facilitating cost-effective and fine-line patterning¹³.

$\text{Ge}_{23}\text{Sb}_7\text{S}_{70}$ film-based waveguides have previously been demonstrated for use in mid-IR chemical sensing, and as a host for PbTe-based photodetection^{12,14}. Their nonlinear optical properties however, have not been studied to date at fiber-based experiments. GeSbS is a chalcogenide which possesses optical transparency far into the mid-IR region, negligible two-photon losses at $1.55\ \mu\text{m}$ and relatively large optical nonlinearities¹⁵. It was previously put forth by Harbold *et al.* that n_2 is dependent on resonance enhancement of the optical bandgap as well as on the lone pair electron concentration between chalcogen and network-forming elements showing the relation as $1/E_g^4$ (E_g = electric bandgap energy)^{16–19}. A similar phenomenon has also been observed in CMOS photonic materials, where the nonlinearity of the films scales inversely with E_g ^{20–23}. In the study on the composition of $\text{Ge}_{23}\text{Sb}_7\text{S}_{70-x}\text{Se}_x$ using X-ray photoelectron spectroscopy²⁴, an increase in Ge-Se bond from 2×10^{-21} to $8 \times 10^{-21}/\text{cm}^3$ results in an increase in the n_2 from 2×10^{-18} to $10 \times 10^{-18}\ \text{m}^2/\text{W}$. Petit *et al.* summarized the composition of the investigated GeSbS chalcogenide glasses at $1.064\ \mu\text{m}$ showing n_2 of $1.7–2.6 \times 10^{-18}\ \text{m}^2/\text{W}$, nonlinear absorption $< 0.1\ \text{cm}/\text{GW}$ and bandgap energy of $1.8–2.3\ \text{eV}$, which in aggregate makes the material a good candidate for applications at telecommunication wavelengths or beyond^{19,25}.

Thanks to wide transparencies and low nonlinear absorptions of chalcogenide materials, a number of studies on supercontinuum generations have been implemented^{126–28}, in particular, the recent researches focus on getting wideband spectra within the mid-IR range^{29–31}. Recently, Yu *et al.* succeeded to fabricate 18-mm-long GeAsSe rib waveguide then to obtain supercontinuum spanning from 2 to $10\ \mu\text{m}$ of wavelength by pumping 330 fs laser with pump wavelength of $\sim 4\ \mu\text{m}$ ³². The potential of on-chip chalcogenide platforms for the generation of wideband spectral broadening using cheaper, more easily available near-IR pumps to realize supercontinuum spectra covering near to mid-IR wavelengths are also of great merit. Within the regime of supercontinuum pumped at the telecommunications wavelength, the dispersion-engineered planar As_2S_3 waveguide has been reported to generate supercontinuum spanning of $750\ \text{nm}$ at $-30\ \text{dB}$ level at TM mode using a 610 fs fiber laser as a pump of $1.55\ \mu\text{m}$ wavelength³³.

In this manuscript, we investigate the nonlinear optical properties of GeSbS including the nonlinear refractive index and nonlinear absorption properties at the shortwave-IR range. Waveguides are also used in nonlinear spectral broadening experiments, and supercontinuum generation extending beyond the $2\ \mu\text{m}$ wavelength is achieved using 500 fs pulses centered at $1.55\ \mu\text{m}$. The results suggest that GeSbS waveguides could also be used successfully for nonlinear optics applications extending to the mid-infrared range, which suggests the potential of the platform to achieve broadening covering both near- and mid-IR range.

Results

The refractive index of $\text{Ge}_{23}\text{Sb}_7\text{S}_{70}$ film (n_{film}) is measured using Fourier transform infrared spectroscopy to be 2.17 at $1.55\ \mu\text{m}$ of wavelength, which depicts a refractive index difference (Δn) of 0.73 between the film and SiO_2 substrate. Figure 1(a) shows the measured n , k values of the $\text{Ge}_{23}\text{Sb}_7\text{S}_{70}$ film. The k -value of the film is observed to be negligible from $600\ \text{nm}$ past $2.5\ \mu\text{m}$. Using Tauc's method, the band gap of the films are extrapolated to be $\sim 2.5\ \text{eV}$. The GeSbS ridge waveguide has a length of $15\ \text{mm}$, a width (W_c) and height (H) of $2\ \mu\text{m}$ and $1.3\ \mu\text{m}$, respectively, as shown in Fig. 1(b). Input and output ports in the waveguide possess tapered couplers with a width (W) of $15\ \mu\text{m}$. W changes linearly into W_c over a distance of $5\ \text{mm}$ from both input and output ports. The length of the straight section of the waveguide with width, W_c is $5\ \text{mm}$. The input tapers facilitate fiber-waveguide coupling. The effective refractive indices of the waveguide (n_{eff}) at quasi-TE mode are calculated using a fully vectorial beam propagation method from RSOFT as shown in Fig. 2(a). n_{eff} ranges from 2.12 to 2.05 at wavelengths between $1.3–1.8\ \mu\text{m}$. Waveguide dispersion (D), derived from n_{eff} values obtained in the simulation program, is $-60\ \text{ps}/\text{nm}/\text{km}$ at $1.55\ \mu\text{m}$ that lies in normal dispersion as shown in Fig. 2(b). Compared with material dispersion ($\sim -240\ \text{ps}/\text{nm}/\text{km}$ at $1.55\ \mu\text{m}$), the waveguide dispersion while still normal, experiences a reduction in the magnitude of dispersion, implying the potential to achieve phase matching for parametric processes by engineering the dispersion. In addition, it implies that the waveguide geometry has somewhat impacted the magnitude of the dispersion though not to the extent available in high index contrast platforms such as silicon on insulator or silicon rich nitride on insulator.

To characterize the nonlinear refractive index of the $\text{Ge}_{23}\text{Sb}_7\text{S}_{70}$ films, self-phase modulation (SPM) experiments are firstly performed with the fabricated GeSbS waveguides. $1.8\ \text{ps}$ pulses adjusted for the transverse-electric polarization with a $20\ \text{MHz}$ repetition rate centered at $1.55\ \mu\text{m}$ are coupled into the waveguide. The spectra of the output TE signals were observed using an optical spectrum analyzer with a measurement range of $1000\ \text{nm}–2400\ \text{nm}$. Experimentally measured SPM-broadened spectra as the input peak power (P_{peak}) is varied

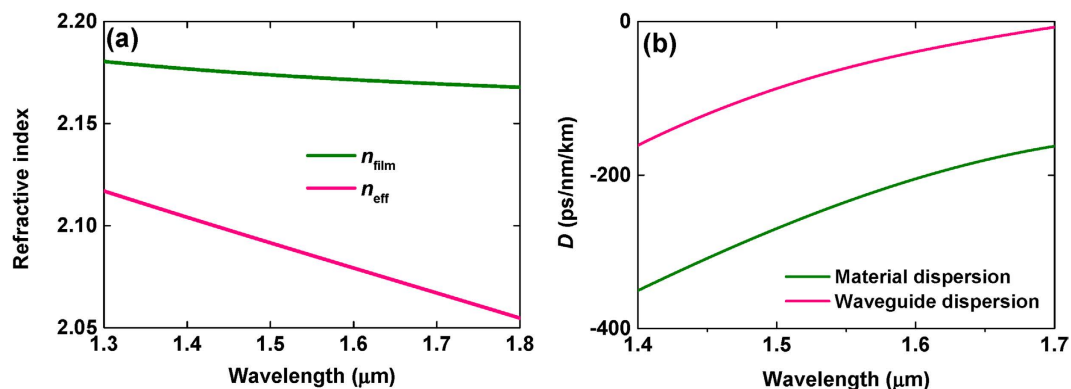


Figure 2. (a) Refractive index of Ge₂₃Sb₇S₇₀ film and effective index of GeSbS waveguide, (b) material and waveguide dispersion (D) calculated from the n value.

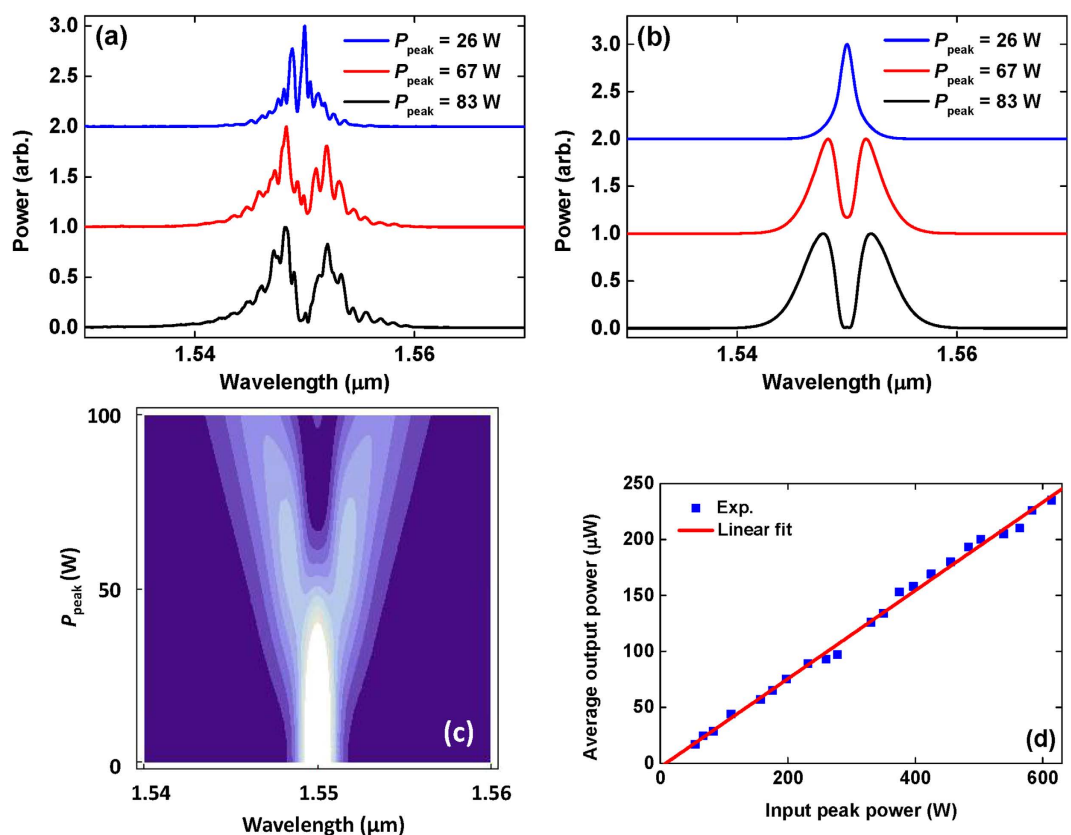


Figure 3. (a) Experimental and (b) theoretical SPM-induced broadened spectra as a function of input peak power, and (c) the evolution of SPM-induced spectra (wavelength-dependent intensity distribution) in terms of input peak power (d) a linear relation between input and output power is observed, implying negligible nonlinear losses.

are shown in Fig. 3(a). Small period oscillations observed in the pulse spectra (Fig. 3(a)) are likely due to Fabry Perot oscillations arising from the effective mirrors created at the input and output tapers. P_{peak} noted in Fig. 3(a) depicts the coupled input peak power compensated for waveguide loss and output fiber-waveguide coupling loss (4.3 dB per facet). The spectral bandwidth at the -30 dB level is 18, 31 and 35 nm at $P_{\text{peak}} = 26, 67$ and 83 W, respectively. The linear increase in the bandwidth as P_{peak} is increased implies that nonlinear loss such as two-photon absorption is negligible as proven by previous reports on GeSbS materials at this wavelength. The nonlinear phase shift φ_{NL} is approximately estimated by the relation as $(M-0.5)\pi$ (M = the number of peaks). $\varphi_{\text{NL}} = 1.5\pi$ is achieved approximately at $P_{\text{peak}} \sim 83$ W.

Using the nonlinear Schrödinger equation, the pulse evolution over the waveguide length as the input peak power is varied is calculated. The modeled pulse evolution as P_{peak} is continuously varied is also presented

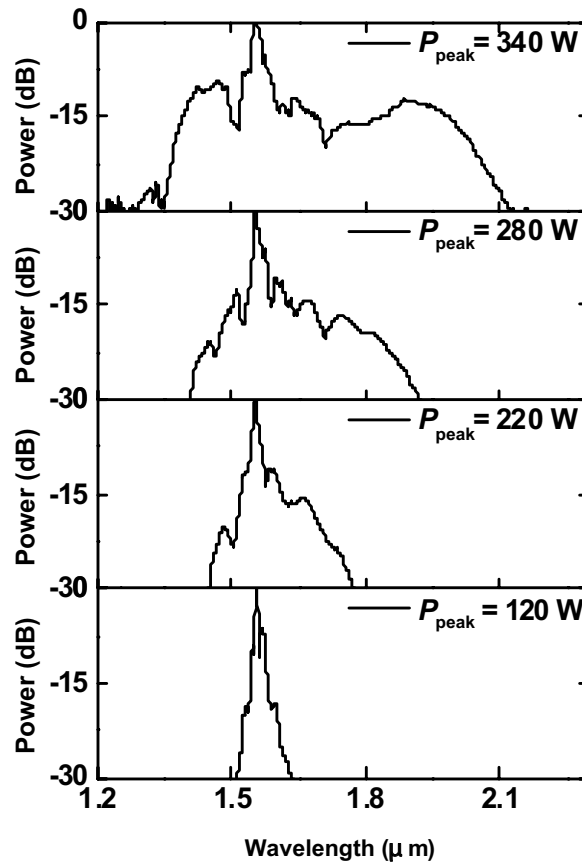


Figure 4. Output supercontinuum spectrum in GeSbS waveguide as a function of input peak power. The output spectrum broadens as input peak power increases up to 340 W.

as Fig. 3(c). It is observed that $\varphi_{NL} \sim 1.5\pi$ appears when $P_{peak} \sim 70\text{--}100$ W. Three peaks are observed when $P_{peak} \sim 100$ W, implying that $1.5\pi < \varphi_{NL} < 2.5\pi$. The nonlinear parameter is extracted using the best fit to the measured experimental data. γ is estimated to be $7\text{ W}^{-1}/\text{m}$ by comparing the experimental and theoretical SPM spectra shown in Fig. 3(a,b). The waveguide's effective area, A_{eff} ³⁴ is calculated to be $2.15\ \mu\text{m}^2$, and is an order of magnitude larger than that available in silicon on insulator waveguides²¹, due to the smaller index difference with the cladding. Further geometric optimization, however, could yield waveguide designs with smaller effective areas and concomitantly, larger values of γ . The nonlinear refractive index (n_2) of the GeSbS film is extracted using the expression, $\gamma = 2\pi n_2 / (\lambda A_{eff})$ to be $3.71 \times 10^{-18}\ \text{m}^2/\text{W}$ at the $1.55\ \mu\text{m}$ wavelength, comparable to that previously measured in microstructured GeSbS fibers ($= 2.8 \times 10^{-18}\ \text{m}^2/\text{W}$)¹⁵. The GeSbS waveguide has fabrication errors of $W_c \pm 50$ nm and $H \pm 10$ nm, which impacts both D and A_{eff} . Since the dispersion length ($L_D = T_0^2/\beta_2$) is much longer than the waveguide length, dispersive effects are negligible compared to the effects of self-phase modulation. Therefore, the uncertainty in D arising from fabrication errors (± 3 ps/nm/km) also has a negligible effect on the uncertainty in γ . The effect of the fabrication uncertainty in A_{eff} ($\pm 0.008\ \mu\text{m}^2$) however translates into an uncertainty in n_2 of $0.02 \times 10^{-18}\ \text{m}^2/\text{W}$ ($\sim 0.5\%$ of the value of n_2).

Nonlinear loss characterization is also performed with the 1.8 ps fiber laser amplified using an erbium-doped fiber amplifier (EDFA). A linear relation between input and output power is measured up to $7\ \text{GW}/\text{cm}^2$, implying the absence of nonlinear losses up to this optical intensity as shown in Fig. 3(d). The onset of two photon absorption (TPA) – induced loss has been reported to occur at intensities exceeding $1\ \text{GW}/\text{cm}^2$ in As – based chalcogenide waveguides such as in Ag–As₂Se₃ chalcogenide photonic crystal waveguides³⁵. Negligible nonlinear losses characterized at this wavelength agree with our characterization of the material's bandgap (Fig. 1); the band gap of 2.5 eV for the Ge₂₃Sb₇S₇₀ films implies a TPA edge at $\sim 1\ \mu\text{m}$. Therefore, our GeSbS waveguides can be efficiently utilized for nonlinear optics applications at the telecommunications wavelength.

The ultrafast spectral broadening in GeSbS is also studied by using a 500 fs fiber laser at a repetition rate of 20 MHz and the evolution of supercontinuum generation as a function of input peak power is shown in Fig. 4. The input laser enters into a GeSbS waveguide with a taper to promote fiber-waveguide coupling. W changes linearly into W_c over a distance of 3.5 mm from the output port. The length of the straight waveguide section with width W_c is 7.5 mm. The spectrum broadens to 130, 320, 510 and 840 nm at -30 dB level for $P_{peak} = 120, 220, 280$ and 340 W, respectively. At the maximum coupled power of 340 W, the spectrum measured at the -30 dB level broadens by a factor of 14. At $P_{peak} = 120$ W, the output spectrum broadens 2 times larger than that in 500 fs fundamental source appearing two sidebands at around 1530 and 1590 nm of wavelength in the vicinity of pump wavelength. Additional two more sidebands at around 1480 and 1660 nm appears at $P_{peak} = 220$ W. Sidebands

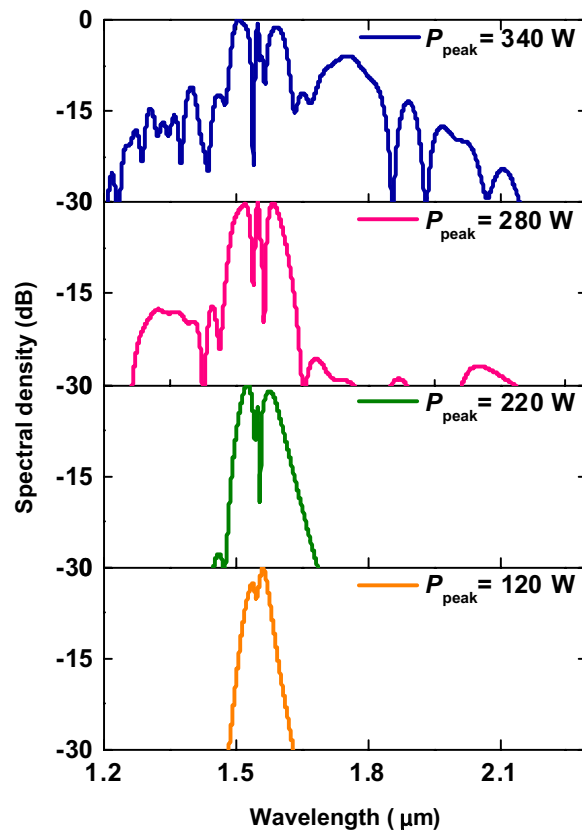


Figure 5. Simulated supercontinuum spectra by input peak power. The nonlinear Schrödinger equation includes GVD, TOD, SPM, self-steepening, and Raman response effects.

at 1450 and 1750 nm are added at $P_{\text{peak}} = 280$ W, and small peaks are shown between two sidebands of 1590 and 1660 nm. At P_{peak} of 340 W, several narrow sidebands appeared at $P_{\text{peak}} < 340$ W are merged, which further evolve into three broad sidebands at around 1450, 1670 and 1930 nm.

In analyzing the supercontinuum generated, SPM alone is insufficient to account for the broadening past 2 μ m. We note further that the waveguide operates in the normal dispersion regime, and therefore nonlinear effects such as soliton fission, cascaded four wave mixing which require anomalous dispersion do not come into play. In previous work, microstructured GeSbS fiber was reported to have a Raman detuning of 9.7 THz and a large Raman gain coefficient of 1.8×10^{-11} m/W¹⁵, 180 times larger than a fused silica fiber³⁶ and 3 times larger than a As₂S₃ fiber³⁷. We predict that stimulated Raman scattering (SRS) is one mechanism contributing to the wideband supercontinuum generation, particularly on the red shifted side of the spectrum. To understand how much the Raman effect influences on the wide spectral output, we simulate supercontinuum generation that includes the terms representing group velocity dispersion (GVD), third order dispersion (TOD), SPM, self-steepening and Raman effects in nonlinear Schrödinger equation³⁴.

The simulated supercontinuum spectra as a function of P_{peak} are shown in Fig. 5. When we set slope of Raman gain (T_R) = 1 ps, the theoretically obtained spectral bandwidth at -30 dB level is 140, 240, 860 and 940 nm at $P_{\text{peak}} = 120, 220, 280$ and 340 W, respectively and matches the experimental data closely. At $P_{\text{peak}} = 220$ W, a slightly spectral asymmetry emerges and a small Raman - induced side lobe appears. At $P_{\text{peak}} = 280$ W, two small peaks around 1.87 and 2.07 μ m emerge at power levels 3 orders of magnitude lower than that in the vicinity of 1.55 μ m. These cannot be experimentally observed as a result of limitations in the sensitivity of the optical spectrum analyzer used to capture the spectrum. Consequently, the experimentally observed spectrum at $P_{\text{peak}} = 280$ W is slightly narrower in bandwidth than the theoretical prediction. Supercontinuum spanning close to an octave and facilitated by cascaded SRS using an input power of 340 W is achieved. The spectrum broadens more extensively along the red - shifted side, and may be accounted for by the cascaded generation of the Stokes lines at wavelengths larger than the input wavelength, as verified from the theoretical curves³⁸. Within our analysis, we expect that the Raman response is a key contributor to the generated supercontinuum. T_R on the chalcogenide waveguide is estimated to be 1 ps, whereas the Raman response time of fused silica is less than 100 fs³⁹. Consequently, the adoption of 500 fs input pulses, shorter than the duration of T_R is likely to contribute to the supercontinuum.

Discussions

Significant progress has been made in nonlinear all - optical signal processing using chalcogenide glasses on integrated waveguide platforms at the telecommunications wavelength. Of these, As₂S₃ and As₂Se₃ have seen the greatest strides⁴⁰⁻⁴³. Specialized methods of synthesizing the glasses and device fabrication are generally the

challenges faced when trying to conduct studies on new chalcogenide materials. Studies on the nonlinear optical properties of GeSbS have so far been limited mainly to bulk or fiber studies¹⁵, and relatively unexplored in integrated platforms. In this study, the Ge₂₃Sb₇S₇₀ film deposition was performed using thermal evaporation from a bulk glass. The high quality of the source glass and deposition process enables the fabricated waveguides to have linear losses which are relatively low, thus facilitating the observation of nonlinear optics phenomena. The use of multi – component materials, such as the Ge – based sulfide glass in this work, allows fabrications flexibility through solution derived glass film processing routes⁴⁴, avoids the use of arsenic, and has shown the ability to add elements to improve rare – earth solubility needed for active chalcogenide glass development⁴⁵. Additionally, thermally deposited GeSbS films have been shown to have outstanding adhesion to SiO₂ substrates, aiding in the fabrication of high quality photonic structures with smooth sidewalls⁴⁶. One key advantage of GeSbS is its very wide transparency window, spanning beyond 12 μm. Consequently, utilization of GeSbS – based waveguides are promising candidates for both linear and nonlinear optical applications from the mid – to long – infrared wavelengths.

Conclusions

In summary, GeSbS waveguides with a length of around 10 mm have been used to characterize their nonlinear optical properties and obtain large spectral broadening at the telecommunications wavelength. SPM broadened spectra using peak powers of up to 83 W are achieved and a nonlinear parameter of 7 W⁻¹/m is extracted. The nonlinear refractive index of the GeSbS films is characterized to be 3.71 × 10⁻¹⁸ m²/W at the 1.55 μm wavelength. The supercontinuum generation exceeding 900 nm is achieved using a peak power of 340 W. This large nonlinear broadening in our GeSbS waveguides may be further enhanced by reducing the waveguide effective area or using even shorter input pulses. Even wider supercontinuum can also be generated using pulses which are ≤ 100 fs in temporal width, which is commonly used in experiments to generate supercontinuum. The relatively large nonlinear parameter and negligible nonlinear losses shown in this paper show that GeSbS waveguides could be a promising platform for nonlinear optics applications at the telecommunications wavelength and beyond.

Methods

Nonlinear Schrödinger equation including Raman effect.

$$\frac{\partial A}{\partial z} = -\frac{\alpha}{2}A - i\frac{\beta_2}{2}\frac{\partial^2 A}{\partial T^2} + \frac{\beta_3}{6}\frac{\partial^3 A}{\partial T^3} + i\left[|A|^2 A + \frac{i}{\omega_0}\frac{\partial}{\partial T}(|A|^2 A) - T_R A \frac{\partial |A|^2}{\partial T}\right] \quad (1)$$

where A and ω_0 are the field amplitude of hyperbolic secant pulse and carrier frequency, respectively. α is loss coefficient of 0.83 cm⁻¹. The partial differential equation is numerically solved by discretizing in all but one dimension and then integrating the semi-discrete problem as a system of ordinary differential equation and differential-algebraic equation. T_R is related to the slope of Raman gain providing the expression as $T_R = \int_0^\infty t R(t) dt$ ($=R(t)$, Raman response function). The shock distance z_s representing self-steepening effect is 5 cm at $P_{\text{peak}} = 340$ W, which is about 2 orders of magnitude larger than L_{NL} at the same peak power. Therefore, self-steepening is unlikely to have a significant effect on the supercontinuum generation. From the calculated dispersion, $\beta_2 = 0.073$ ps²/m and $\beta_3 = 6.42 \times 10^{-4}$ ps³/m at 1.55 μm.

Device fabrication. GeSbS waveguides are fabricated on Si substrates with a 3 μm thick thermal oxide layer. NR9 photoresist is first spincoated and the waveguides are patterned into the photoresist using a mask aligner. Ge₂₃Sb₇S₇₀ film is then deposited on the patterned substrate using a thermal evaporator. Finally, the photoresist is lifted off in acetone.

References

- Slusher, R. E. *et al.* Large Raman gain and nonlinear phase shifts in high-purity As₂Se₃ chalcogenide fibers. *J. Opt. Soc. Am. B* **21**, 1146–1155 (2004).
- Asobe, M. Nonlinear optical properties of chalcogenide glass fibers and their Application to all-optical switching. *Opt. Fiber. Technol.* **3**, 142–148 (1997).
- Saliminia, A., Villeneuve, A., Galstyan, T. V., LaRochelle, S. & Richardson, K. First- and second-order Bragg gratings in single-mode planar waveguides of chalcogenide glasses. *J. Lightwave Technol.* **17**, 837–842 (1999).
- Asobe, M., Ohara, T., Yokohama, I. & Kaino, T. Low power all-optical switching in a nonlinear optical loop mirror using chalcogenide glass fibre. *Electron Lett.* **32**, 1396–1397 (1996).
- Fu, L., Rochette, M., Tåeéd, V. G., Moss, D. J. & Eggleton, B. J. Investigation of self-phase modulation based optical regeneration in single mode As₂Se₃ chalcogenide glass fiber. *Opt. Express* **13**, 7637–7643 (2005).
- Tåeéd, V. G. *et al.* Integrated all-optical pulse regenerator in chalcogenide waveguides. *Opt. Lett.* **30**, 2900–2902 (2005).
- Wei, D.-P., Galstian, T. V., Smolnikov, I. V., Plotnichenko V. G. & Zohrabyan, A. Spectral broadening of femtosecond pulses in a single-mode As-S glass fiber. *Opt. Express* **13**, 2439–2443 (2005).
- Fuxi, G. Structure, properties and applications of chalcogenide glasses: a review. *J. Non-Cryst. Solids* **140**, 184–193 (1992).
- Vahalová, R., Tichý, L., Vlček, M. & Tichá, H. Far infrared spectra and bonding arrangement in some Ge–Sb–S glasses. *Phys. Status Solidi A* **181**, 199–209 (2000).
- Petit, L. Correlation between physical, optical and structural properties of sulfide glasses in the system Ge–Sb–S. *Mater. Chem. Phys.* **97**, 64–70 (2006).
- Asami, T., Matsuishi, K., Onari, S. & Arai, T. Low frequency Raman scattering spectra of (GeS₂)_{1-x}(Sb₂S₃)_x amorphous semiconductors. *J. Non-Cryst. Solids* **211**, 89–94 (1997).
- Singh, V. *Chalcogenide Glass Materials for Integrated Infrared Photonics*. (Ph.D. thesis in Massachusetts Institute of Technology, 2015).
- Hu, J. *et al.* Si-CMOS-compatible lift-off fabrication of low-loss planar chalcogenide waveguides. *Opt. Express* **15**, 11798–11807 (2007).
- Han, Z. *et al.* On-chip mid-infrared gas detection using chalcogenide glass waveguide. *Appl. Phys. Lett.* **108**, 141106 (2016).

15. Fatome, J. *et al.* Linear and nonlinear characterizations of chalcogenide photonic crystal fibers. *J. Lightwave Technol.* **27**, 1707–1715 (2009).
16. Harbold, J. M., Ilday, F. Ö., Wise, F. W. & Aitken, B. G. Highly Nonlinear Ge–As–Se and Ge–As–S–Se glasses for all-optical switching. *IEEE Photon. Technol. Lett.* **14**, 822–824 (2002).
17. Sheik-Bahae, M., Hagan, D. J. & Van Stryland, E. W. Dispersion and band-gap scaling of the electronic Kerr effect in solids associated with two-photon absorption. *Phys. Rev. Lett.* **65**, 96–99 (1990).
18. Tanaka, K. Nonlinear optics in glasses: How can we analyze?. *J. Phys. Chem. Solids* **68**, 896–900 (2007).
19. Petit, L. *et al.* Compositional dependence of the nonlinear refractive index of new germanium-based chalcogenide glasses. *J. Solid State Chem.* **182**, 2756–2761 (2009).
20. Wang, T. *et al.* Supercontinuum generation in bandgap engineered, back-end CMOS compatible silicon rich nitride waveguides. *Laser Photon. Rev.* **9**, 498–506 (2015).
21. Tan, D. T. H., Sun, P. C. & Fainman, Y. Monolithic nonlinear pulse compressor on a silicon chip. *Nat. Commun.* **1**, 116 (2010).
22. Tan, D. T. H., Ikeda, K., Sun, P. C. & Fainman, Y. Group velocity dispersion and self phase modulation in silicon nitride waveguides. *Appl. Phys. Lett.* **96**, 061101 (2010).
23. Moss, D. J., Morandotti, R., Gaeta, A. L. & Lipson, M. New CMOS-compatible platforms based on silicon nitride and Hydex for nonlinear optics. *Nat. Photon.* **7**, 597–607 (2013).
24. Petit, L. *et al.* Correlation between the nonlinear refractive index and structure of germanium-based chalcogenide glasses. *Mater. Res. Bull.* **42**, 2107–2116 (2007).
25. Petit, L. *et al.* Nonlinear optical properties of glasses in the system Ge/Ga–Sb–S/Se. *Opt. Lett.* **31**, 1495–1497 (2006).
26. Yeom, D.-I. *et al.* Low-threshold supercontinuum generation in highly nonlinear chalcogenide nanowires. *Opt. Lett.* **33**, 660–662 (2008).
27. Hu, J., Menyuk, C. R., Shaw, L. B., Sanghera, J. S. & Aggarwal, I. D. Maximizing the bandwidth of supercontinuum generation in As₂Se₃ chalcogenide fibers. *Opt. Express* **18**, 6722–6739 (2010).
28. Marandi, A. *et al.* Mid-infrared supercontinuum generation in tapered chalcogenide fiber for producing octave-spanning frequency comb around 3 μm. *Opt. Express* **20**, 24218–24225 (2012).
29. Yu, Y. *et al.* A broadband, quasi-continuous, mid-infrared supercontinuum generated in a chalcogenide glass waveguide. *Laser Photon. Rev.* **8**, 792–798 (2014).
30. Gao, W. *et al.* Mid-infrared supercontinuum generation in a suspended-core As₂S₃ chalcogenide microstructured optical fiber. *Opt. Express* **21**, 9573–9583 (2013).
31. Domachuk, P. *et al.* Over 4000 nm bandwidth of mid-IR supercontinuum generation in sub-centimeter segments of highly nonlinear Tellurite PCFs. *Opt. Express* **16**, 7161–7168 (2008).
32. Yu, Y. *et al.* Experimental demonstration of linearly polarized 2–10 μm supercontinuum generation in a chalcogenide rib waveguide. *Opt. Lett.* **41**, 958–961 (2016).
33. Lamont, M. R. E., Luther-Davies, B., Choi, D.-Y., Madden, S. & Eggleton, B. J. Supercontinuum generation in dispersion engineered highly nonlinear ($\gamma = 10/W/m$) As₂S₃ chalcogenide planar waveguide. *Opt. Express* **16**, 14938–14944 (2008).
34. Agrawal, G. P. *Nonlinear Fiber Optics* (Academic, 1995).
35. Suzuki, K. & Baba, T. Nonlinear light propagation in chalcogenide photonic crystal slow light waveguides. *Opt. Express* **18**, 26675–26685 (2010).
36. Fortier, C. *et al.* Experimental investigation of Brillouin and Raman scattering in a 2SG sulfide glass microstructured chalcogenide fiber. *Opt. Express* **16**, 9398–9404 (2008).
37. Kulkarni, O. P. *et al.* Third order cascaded Raman wavelength shifting in chalcogenide fibers and determination of Raman gain coefficient. *Opt. Express* **14**, 7924–7930 (2006).
38. Qiu, Y., Xu, Y. Q., Wong, K. K. Y. & Tsia, K. K. Enhanced supercontinuum generation in the normal dispersion pumping regime by seeded dispersive wave emission and stimulated Raman scattering. *Opt. Commun.* **325**, 28–34 (2014).
39. Stolen, R., Gordon, J. P., Tomlinson, W. J. & Haus, H. A. Raman response function of silica-core fibers. *J. Opt. Soc. Am. B* **6**, 1159–1166 (1989).
40. Rangel-Rojo, R. *et al.* Near-infrared optical nonlinearities in amorphous chalcogenides. *Opt. Commun.* **109**, 145–150 (1994).
41. Cardinal, T. *et al.* Non-linear optical properties of chalcogenide glasses in the system As-S-Se. *J. Non-Cryst. Solids* **256&257**, 353–360 (1999).
42. Ruan, Y. *et al.* Large phase shifts in As₂S₃ waveguides for all-optical processing devices. *Opt. Lett.* **30**, 2605–2607 (2005).
43. Petersen, C. R. *et al.* Mid-infrared supercontinuum covering the 1.4–13.3 μm molecular fingerprint region using ultra-high NA chalcogenide step-index fibre. *Nat. Photon.* **8**, 830–834 (2014).
44. Song, S. *et al.* Spin-coating of Ge₂₃Sb₇S₇₀ chalcogenide glass thin films. *J. Non-Cryst. Solids* **355**, 2272–2278 (2009).
45. Petit, L. *et al.* Effect of the substitution of S for Se on the structure and non-linear optical properties of the glasses in the system Ge_{0.18}Ga_{0.05}Sb_{0.07}S_{0.70-x}Se_x. *J. Non-Cryst. Solids* **352**, 5413–5420 (2006).
46. Hu, J. *et al.* Planar waveguide-coupled, high-index-contrast, high-Q resonators in chalcogenide glass for sensing. *Opt. Lett.* **33**, 2500–2502 (2008).

Acknowledgements

This work was supported by the MOE ACRF Tier 2 grant, A*STAR PSF grant, SUTD – MIT International Design center and Temasek Laboratories grant. The authors acknowledge the National Research Foundation, Prime Minister's Office, Singapore, under its Medium Sized Centre Program.

Author Contributions

J.W.C. and G.F.R.C. performed experimental characterization. Z.H. and C.S. performed materials growth, characterization and device fabrication. B.-U.S. and J.W.C. performed simulations. J.W.C. and D.T.H.T. analyzed the experimental data. J.W.C. wrote the manuscript with contributions from D.T.H.T. All authors contributed to the manuscript. D.T.H.T., A.M.A., L.C.K. and K.C.R. supervised the project.

Additional Information

Competing financial interests: The authors declare no competing financial interests.

How to cite this article: Choi, J. W. *et al.* Nonlinear characterization of GeSbS chalcogenide glass waveguides. *Sci. Rep.* **6**, 39234; doi: 10.1038/srep39234 (2016).

Publisher's note: Springer Nature remains neutral with regard to jurisdictional claims in published maps and institutional affiliations.



This work is licensed under a Creative Commons Attribution-NonCommercial-NoDerivs 4.0 International License. The images or other third party material in this article are included in the article's Creative Commons license, unless indicated otherwise in the credit line; if the material is not included under the Creative Commons license, users will need to obtain permission from the license holder to reproduce the material. To view a copy of this license, visit <http://creativecommons.org/licenses/by-nc-nd/4.0/>

© The Author(s) 2016